Supplementary Materials - Appendix A

The crystallization of Mercury's magma ocean and the formation of its primordial mantle structure

Fabrizio Saracino, Bernard Charlier, Yishen Zhang, Olivier Namur

Index

S.1 Parameters for the calculation of density of S-free liquids and minerals 3
S.2 The forsterite-enstatite cotectic 5
S.3 Cell assemblies 6
S.4 Composition of silicate melt and metals in time series experiments 7
S.5 Composition of experimentally determined silicate melts 8
S.6 Composition of experimental pyroxenes 9
S.7 Equations for the calculation of the liquidus, solidus temperatures 10
S.8 Cotectic proportions 12
S.9 Crystallization sequence as a function of temperature 13
S. 10 Equations for the calculation of mineral compositions 14
S.11 Lithology of the cumulate pile 15
S.12 Calculation of S-free and S-bearing MMO liquid densities 16
S.13 HPE partitioning in the MMO 18
References 19

S.1 Parameters for the calculation of density of S-free liquids and minerals

Here below is a list with all the partial molar volumes, thermal expansion, Young modulus, and pressure derivative of the Young modulus of the MMO liquid. V_i values are from Lange and Carmichael (1987), Bottinga et al. (1983), Warren (1995). dV_i/dT data are from Lange and Carmichael (1987), Warren (1995).

[SiO_2, TiO_2, Al_2O_3, Cr_2O_3, FeO, MnO, MgO, CaO, Na_2O, K_2O]

V_i = [26.90, 24.60, 37.63, 31.40, 14.23, 14.13, 11.98, 17.15, 30.26, 48.22 [m^3mol^{-1}]

dV_i/dT = [0.00, 7.24, 2.62, 4.40, 2.92, 2.62, 2.62, 2.92, 7.41, 11.91] [$x10^9$ $m^3mol^{-1}K^{-1}$]

K = [5.1485, 29.518, 0.28658, 1.0456, -0.20818, -1.3441, -4.4982] [GPa]

dK/dP = [3.387, -4.3588, -0.049056, -0.28022, 0.13524, 0.47933, 1.3291]

Table S1*: List of physical and volumetric EOS parameters for the solid phases as modelled in our MMO crystallization code. (a)Bertka and Fei (1998) (b) Holland and Powell (1998) (c) Lange and Carmichael (1987) (d) Toplis et al. (1994) (e) Fei et al. (1990) (f) Niu and Batiza (1991) (g) Kosinski (1992) (h) Frondel (1962) (i) Peiris et al. (1994) (j) Baldwin and Tompson (1964).*

	ρ (1atm, 298K; kg / m^3)	α_0 (/K)	α_1 ($x10^{-5}$) (/K)	α_2 ($x10^{-9}$) (/K)	Ref.
Forsterite	3223	3.034	7.422	-0.5381	a,b,c,d
Enstatite	3204	2.947	2.694	-0.5588	c,d,e
Diopside	3272	3.330	2.694	-0.5588	a,c,d
Anorthite	2762	4.560	-	-	b,c,d,f
Albite	2611	2.380	-	-	b,c,d,f
Quartz	2671	1.310	0.002	-0.0606	b,g,h
MgS	2661	6.00E-05	-	-	i,j

	K_T (298K) (GPa)	δK / δP	δK / δT (Gpa/K)	V0 (cm^3/mol)	Ref.
Forsterite	127.1	5.39	-0.0239	43.60	a,b,c,d
Enstatite	107.0	5.00	-0.0270	62.67	c,d,e
Diopside	113.0	4.50	-0.0200	66.04	a,c,d
Anorthite	94.3	4.00	-0.0200	100.43	b,c,d,f
Albite	69.9	4.00	-0.0200	100.38	b,c,d,f
Quartz	96.0	8.40	-0.0200	20.64	b,g,h
MgS	78.9	3.71	-0.0200	21.18	i,j

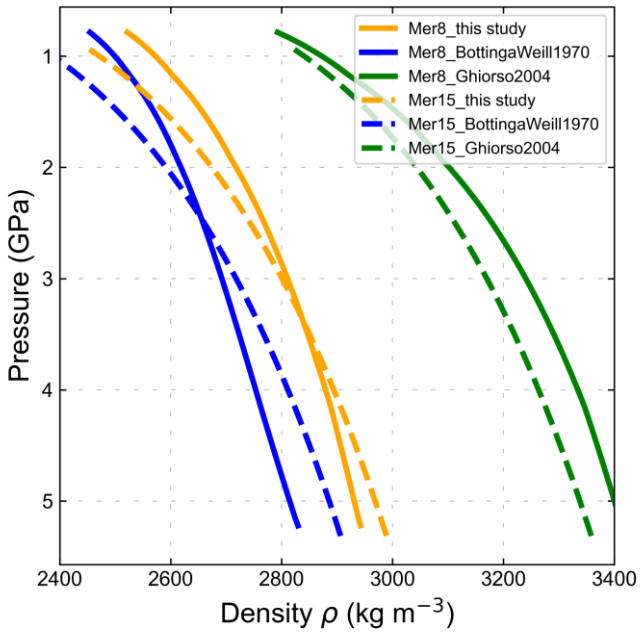

Figure S1: *Density of the residual liquid of the MMO for both Mer8 (solid lines) and Mer15 (dashed lines) using different equations of state (EOS) from this study (orange), Bottinga and Weill (1970) (blue) and Ghiorso (2004) (green). All density calculations here displayed do not consider the effect of sulfur on liquid density.*

S.2 The forsterite-enstatite cotectic

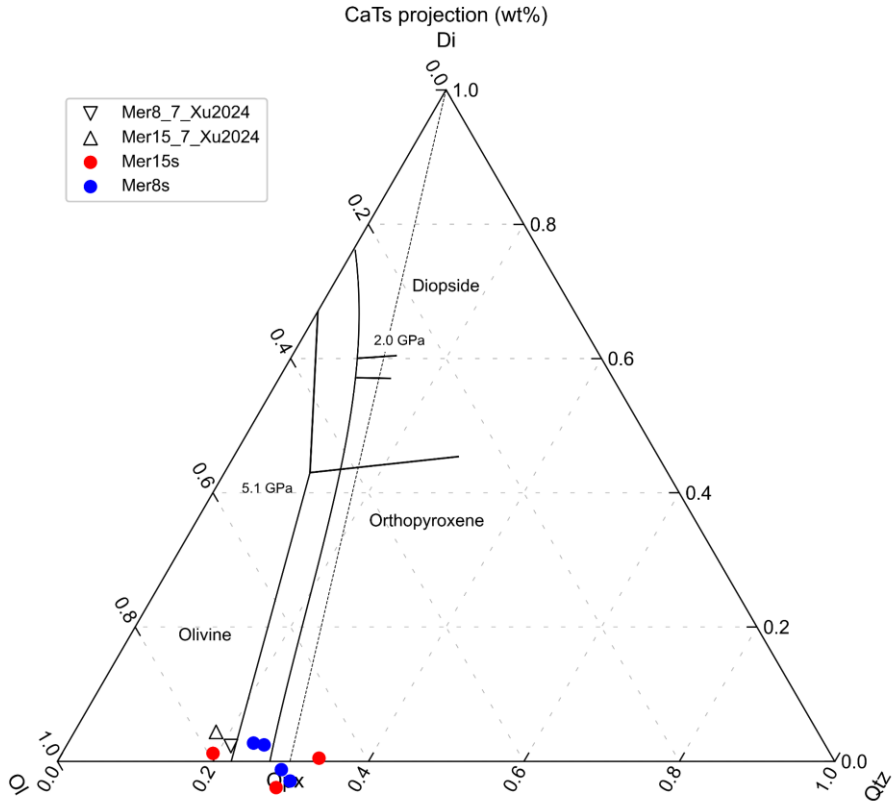

Figure S2: *Diopside-SiO_2-olivine system showing the experimental melts of Mercury's mantle compositions from Saracino et al. (2025) (circles) and Xu et al. (2024) (triangles). The silicate melts were renormalized to take into account the effect of S on the distribution of MgO, and CaO between silicate and sulfide melts (more details are in Saracino et al., 2025). Also shown are the olivine-orthopyroxene boundaries at 5.1 GPa (Weng and Presnall, 2001), and 2 GPa (Kushiro, 1969).*

S.3 Cell assemblies

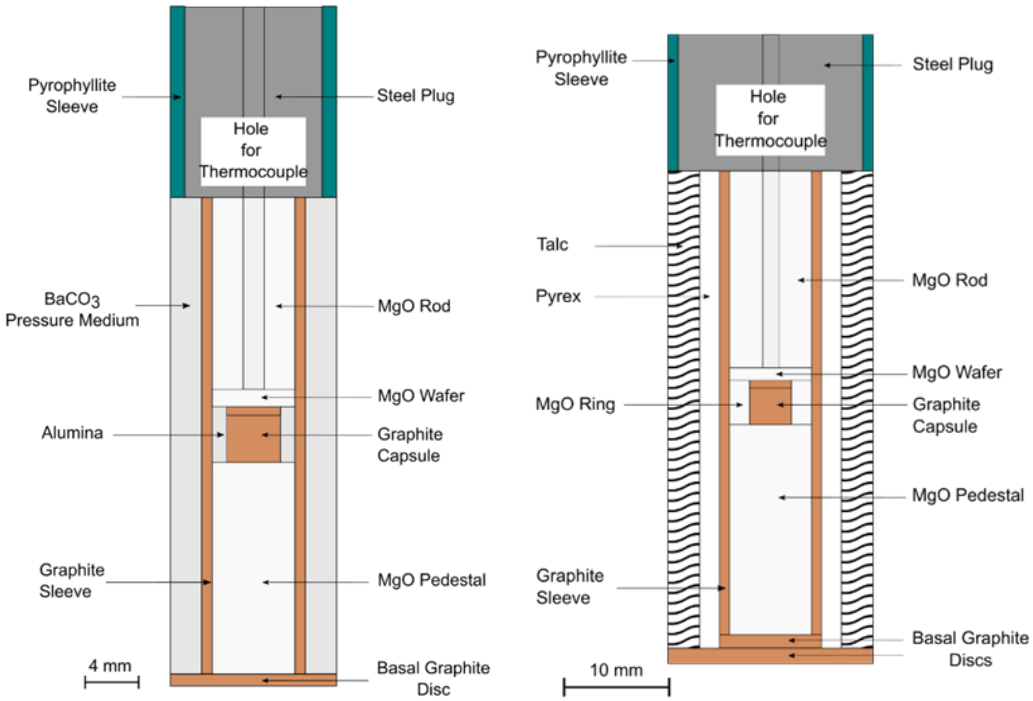

Figure S3: *Two-dimensional sketch of the ½'' and the ¾'' experimental assemblies employed in this study.*

S.4 Composition of silicate melt and metals in time series experiments

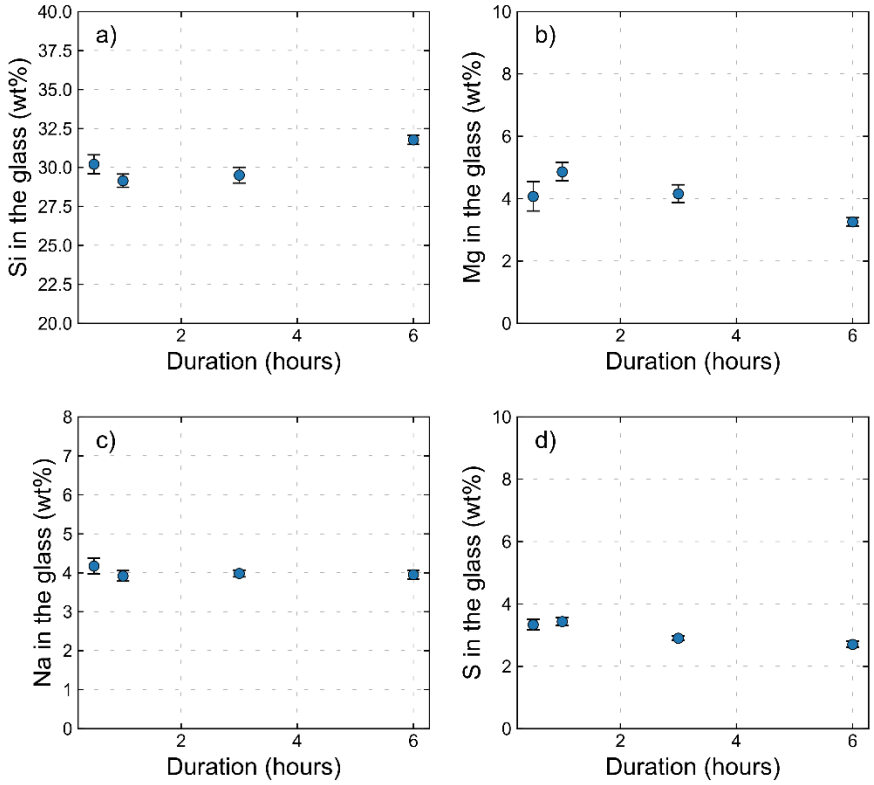

Figure S4: *Major element variation (in wt%) in time series experiments as a function of the experimental duration (in hours).*

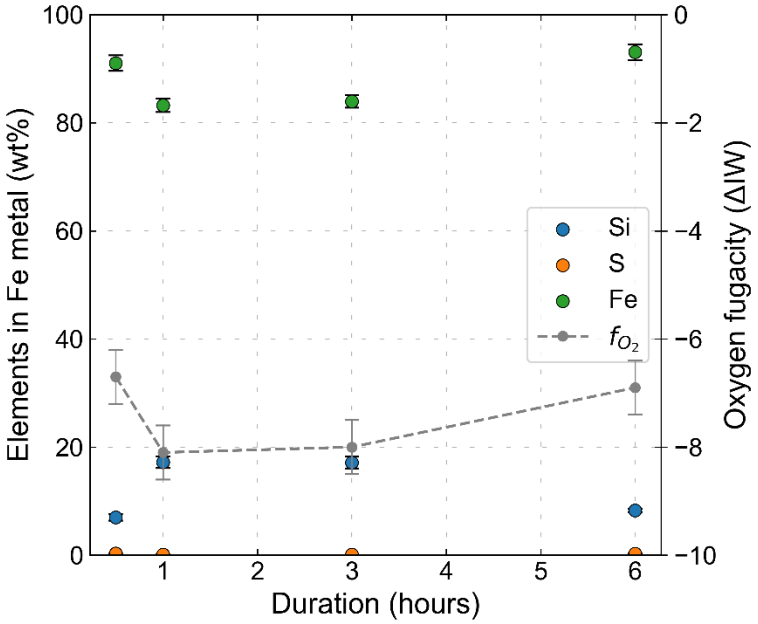

Figure S5: *Variation of Fe, S, and Si in Fe metal (expressed in wt%) in time series experiments as a function of the experimental duration (in hours). Also shown is the variation of calculated oxygen fugacity (relative to IW) as a function of duration.*

S.5 Composition of experimentally determined silicate melts

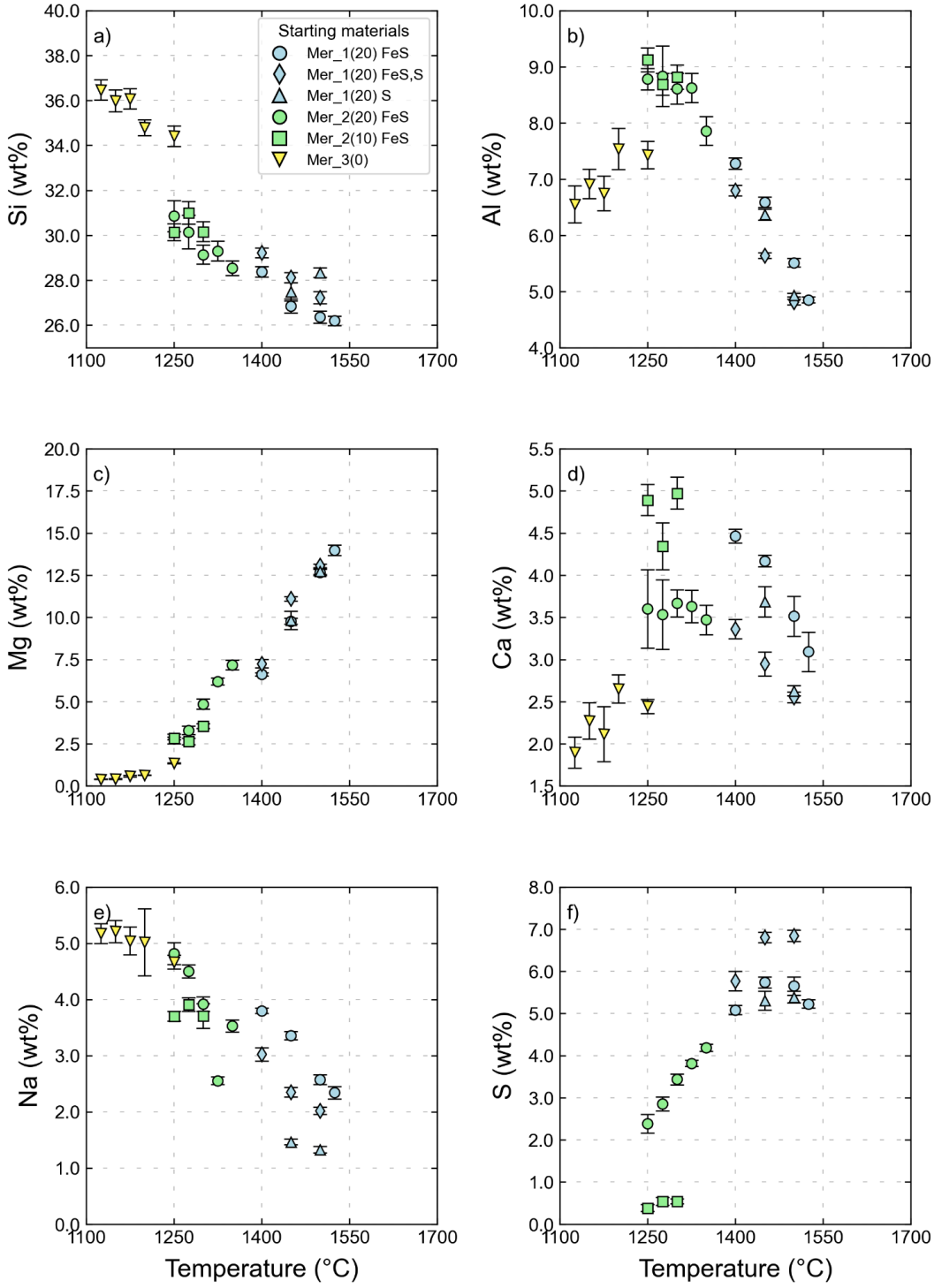

Figure S6: *Evolution of element concentrations (wt%) in the silicate glass as a function of temperature (°C). Vertical bars refer to the 1σ standard deviation of analyses (small 1σ values are hidden by symbols).*

S.6 Composition of experimental pyroxenes

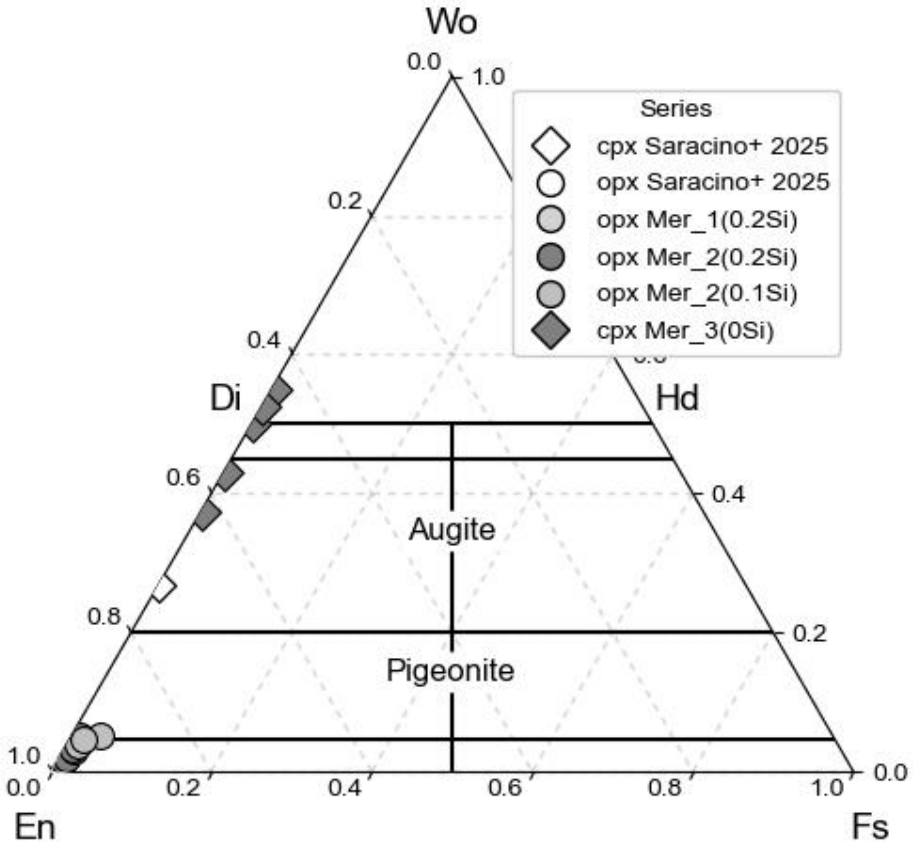

Figure S7: *Pyroxene ternary system (in wt%) showing the composition of orthopyroxene and clinopyroxene crystals in our suite of experiments. Also shown as comparison are the orthopyroxene and clinopyroxene crystals measured in 1.5 GPa and 3.0 GPa experiments on Mer8 and Mer15 compositions in Saracino et al. (2025). Abbreviations: opx – orthopyroxene, cpx – clinopyroxene.*

S.7 Equations for the calculation of the liquidus, solidus temperatures

The thermometer used to calculate the temperature of the MMO at each incremental step of crystallization is based on S-free experimental runs featured in Charlier et al. (2013), Namur and Charlier (2017), Namur et al. (2016), and Saracino et al. (2025) (N=89). The resulting equation is the following (Fig. S2):

$$T_{\text{Liquidus,S-free}} = 858.78 + 105.43\ P\ (GPa) + 18.42\ [MgO] + 13.23\ [Al_2O_3] + 3.71[Na_2O + K_2O]$$

Where *T* is the temperature expressed in °C, *P* is the pressure in GPa, and the oxide concentrations are expressed as wt%. The fit achieves an R^2 of 0.95 (adjusted R^2 = 0.95) and the SEE is 45 °C. After calculating the S-free liquidus temperature at each increment, we applied a correction to account for the influence of S as in Eq. 10 of Saracino et al. (2025):

$$\Delta T_{\text{Liquidus}}(°C) = 8.65\ [S]_{\text{Melt}} + 4.89\ [S]^2_{\text{Melt}} - 0.39\ [S]^3_{\text{Melt}}$$

Where ΔT (°C) is the liquidus temperature depression, and $[S]_{\text{Melt}}$ is the concentration of sulfur in the melt (wt%). The corrected liquidus temperature can now be calculated as such:

$$T_{\text{Liquidus,S-bearing}}(°C) = T_{\text{Liquidus,S-free}}(°C) - \Delta T_{\text{Liquidus}}(°C)$$

A comparison between the uncorrected (S-free) and the corrected (S-bearing) temperatures is shown in Fig. S3. The solidus temperature was derived by fitting the solidus temperatures of our S-free evolving MMO liquid as determined with MAGEMin (Riel et al., 2022) using the 'igneous' database of Holland et al. (2018). The temperature is calculated as follows:

$$T_{\text{Solidus}}(°C) = 864.30 + 222.41\ P(GPa) - 7.77\ P\ (GPa)^2$$

Where *P* is the pressure (in GPa). The fit achieves an R^2 of 0.99 and the SEE is 34 °C. To retrieve the actual solidus temperature, the effect of S on the solidus temperature is needed. To our knowledge, no study focused on quantitatively determining the solidus depression as a function of the sulfur content in reduced silicate melts relevant to Bulk Silicate Mercury (BSMe). As a first approximation, we can therefore apply the same ΔT for the liquidus temperature following the approach of Katz et al. (2003) for H_2O (Fig. S3).

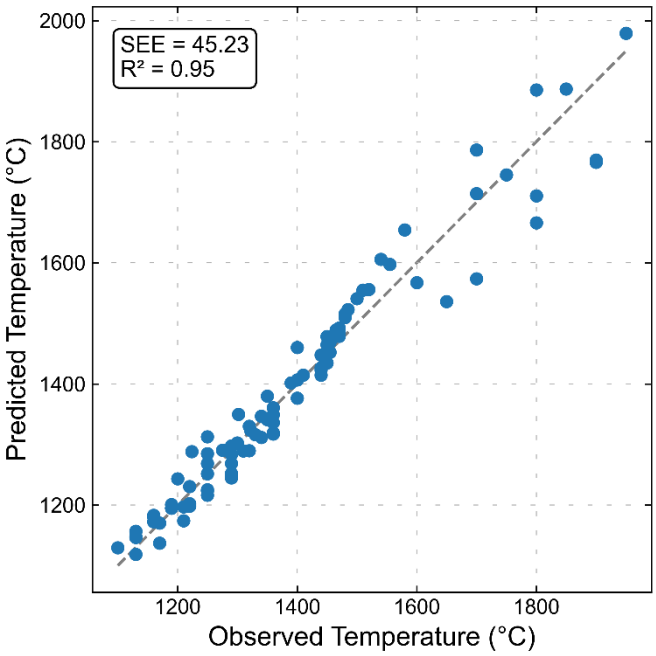

Figure S8: *Calculated versus measured temperatures of Mercury-like mantle compositions. The dataset is from Saracino et al. (2025), Charlier et al. (2013), Namur and Charlier (2017), Namur et al. (2016a). The fit achieves an R^2 of 0.95 and a Standard Error of Estimate (SEE) of 45 °C (N=89). The oxide concentrations are expressed in wt%.*

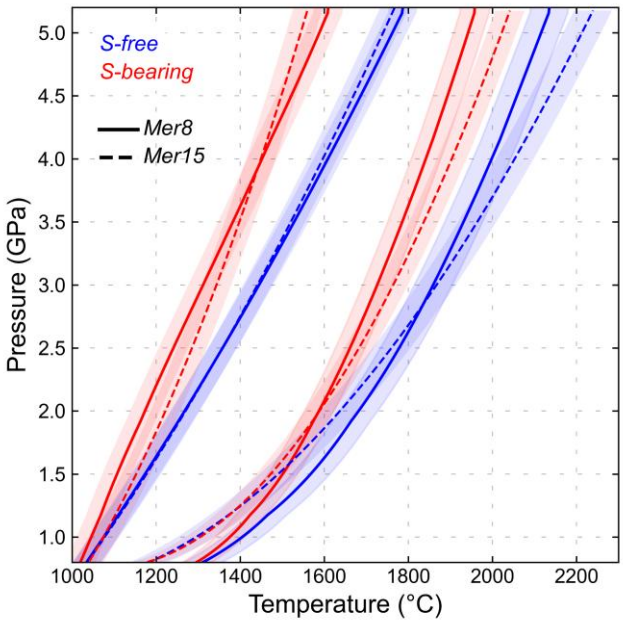

Figure S9: *Comparison between the uncorrected, S-free liquidus temperature (blue line) calculated with Mercury's mantle thermometer, and the corrected, S-bearing liquidus temperature (red line) for both Mer8 (solid lines) and Mer15 (dashed lines). Also shown as comparison is the S-free and S-bearing solidus temperature. The colored areas alongside the curves represent the Standard Errors of Estimate (SEE) of each expression as estimated in this study ($T_{Liquidus,\ S\text{-}free}$) and in Saracino et al. (2025) ($\Delta T_{Liquidus}$).*

S.8 Cotectic proportions

Table S2: *Cotectic proportions used for the MMO crystallization modelling with sulfide-bearing (a) Mer8 and (b) Mer15 starting compositions, respectively.*

(a) Mer8 + (Mg,Ca)S

Cumulus assemblage (wt%)	Fo	En	Cpx	Qtz	Pl	(Mg,Ca)S
En		90				10
En, Fo	22	68				10
En, Fo, Cpx	12	68	10			10
En, Fo, Cpx, Qtz	10	50	25	5		10
En, Cpx, Qtz		35	40	15		10
Cpx, Qtz, Pl			27	18	45	10

(b) Mer15 + (Mg,Ca)S

Cumulus assemblage (wt%)	Fo	En	Cpx	Qtz	Pl	(Mg,Ca)S
Fo	90					10
En, Fo	22	68				10
En, Fo, Cpx	12	68	10			10
En, Fo, Cpx, Qtz	10	50	25	5		10
En, Cpx, Qtz		35	40	15		10
Cpx, Qtz, Pl			27	18	45	10

S.9 Crystallization sequence as a function of temperature

Table S3: *Input range of temperature (°C) used to compute the MMO evolution for Mer8 and Mer15, respectively. Abbreviations: Fo – forsterite, En– enstatite, Cpx – clinopyroxene, Qtz – quartz, Pl – plagioclase.*

Cumulus assemblage	Mer8	Mer15
En / Fo	> 1850 (En)	> 1540 (Fo)
En, Fo	1850 < T < 1575	1540 < T < 1500
En, Fo, Cpx	1575 < T < 1425	1500 < T < 1375
En, Fo, Cpx, Qtz	1425 < T < 1275	1375 < T < 1275
En, Cpx, Qtz	1275 < T < 1250	1275 < T < 1250
Cpx, Qtz, Pl	T < 1250	T < 1250

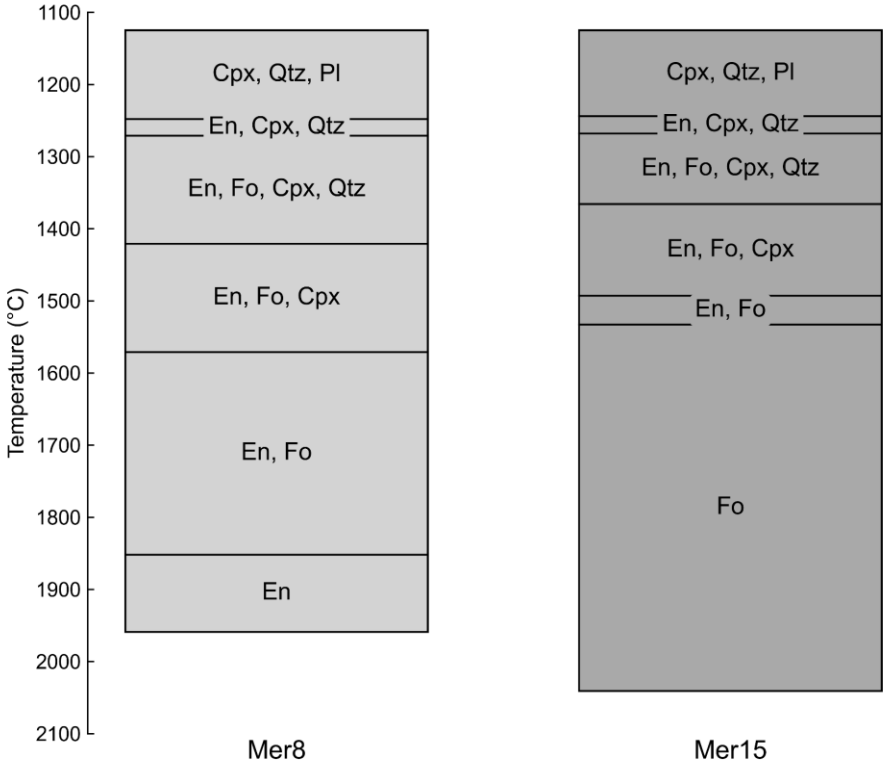

Figure S10: *Crystallization sequence as a function of temperature (°C) for our two sulfide-bearing Mer8 and Mer15. Abbreviations: Fo – forsterite, En – enstatite, Cpx – clinopyroxene, Qtz – quartz, Pl – plagioclase.*

S.10 Equations for the calculation of mineral compositions

Olivine

- Fo = 1
- Al_2O_3 = -0.198 + 0.00009**T* + 0.02398**P* + 0.01221*$Al_2O_{3\ Liq}$ (R^2 = 0.81; SEE = 0.019) (wt%)
- CaO = -0.09 + 0.00006**T* + 0.00181**P* + 0.01183*CaO_{Liq} (R^2 = 0.83; SEE = 0.006) (wt%)
- MnO = 0.05 wt%

Orthopyroxene

- En = 1
- Na_2O, K_2O, P_2O_5 = 0 wt%
- CaO = 1.871 + 0.29504*CaO_{Liq} - 0.00128**T* + 0.20994**P* (R^2 = 0.80; SEE = 0.06) (wt%)
- TiO_2 = 0.05 wt%
- Al_2O_3 = 17.482 - 0.00404*$Al_2O_{3\ Liq}$ + 1.87433**P* – 0.01236**T* (R^2 = 0.90; SEE = 0.35) (wt%)
- MnO = 0.07 wt%

Clinopyroxene

- FeO, Na_2O, K_2O, P_2O_5 = 0 wt%
- MgO = 15.46 wt%
- SiO_2 = 50.00 wt%
- CaO = 4.00 wt%
- TiO_2 = 0.09 wt%
- Al_2O_3 = 7.12 wt%
- MnO = 0.33 wt%

Quartz

- SiO_2 = 100.00 wt%

Plagioclase

- SiO2 = 50.03 wt%
- Al_2O_3 = 33.49 wt%
- CaO = 10.49 wt%
- Na_2O = 5.00 wt%

S.11 Lithology of the cumulate pile

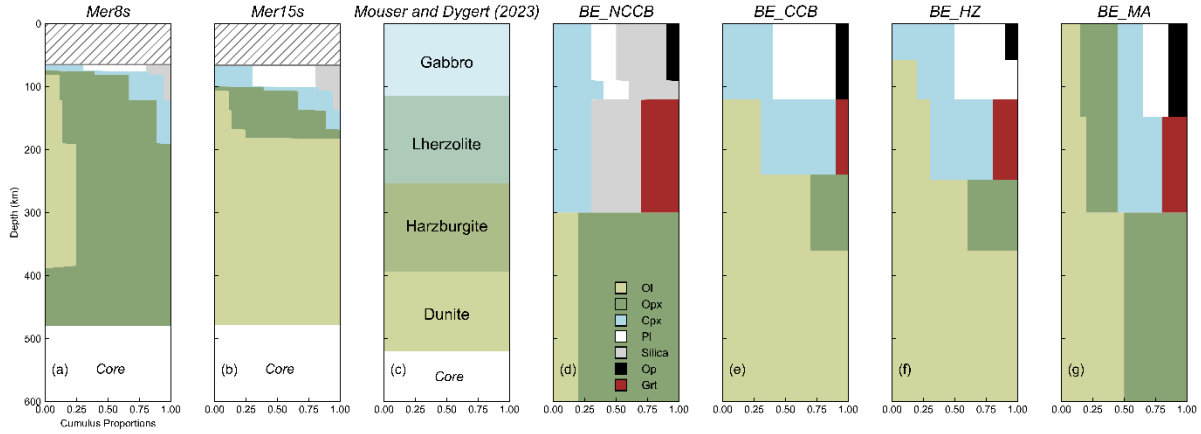

Figure S11: *Comparison of MMO crystallization sequence models (depths are not scaled). (a) Mer8 and (b) Mer15 are from this study. Dashed regions represent parts of the crystallization sequence not modelled in this study; (c) pre-mantle overturn crystallization sequence of Mouser and Dygert (2023) (d) Starting CB chondrite composition (Weisberg et al., 2000; Lauretta et al., 2007) with non-chondritic Si/Mg from Brown and Elkins-Tanton (2009) (e) Starting CB chondrite (Weisberg et al., 2000, 2001; Lauretta et al., 2007) with chondritic Si/Mg from Brown and Elkins-Tanton (2009) (f) Starting Earth's mantle composition based on measurements of fertile lherzolites (Hart and Zindler, 1986) from Brown and Elkins-Tanton (2009) (g) Model composition of Earth calculated from nebular condensation model (Morgan and Anders, 1980) from Brown and Elkins-Tanton (2009). The thicker mantle in the models of Brown and Elkins-Tanton (2009) is based on an old configuration of the interior where a ~ 1800 km-core radius is considered (Riner et al., 2008). Abbreviations: Ol, olivine; Opx, orthopyroxene; Cpx, clinopyroxene; Silica, SiO_2 phases; Pl, plagioclase; Op, opaques; Grt, garnet.*

S.12 Density calculation for sulfur-bearing liquids

To investigate the effect of sulfur on the density of silicate liquids, first we calculated the density of the MMO both in S-free and S-bearing conditions following the method of Bottinga and Weill (1970). Volumetric properties of both elemental S and sulfide phases are not well constrained in the literature, so some approximations were necessary. At room temperature, solid S has a molar volume of ~ 15.5 $cm^3\ mol^{-1}$ (Singman, 1984; Robie and Hemingway, 1995). Sulfides like troilite (FeS), alabandite (MnS), niningerite (MgS), and oldhamite (CaS) have molar volumes in the range 18 - 28 $cm^3\ mol^{-1}$ (Robie and Hemingway, 1995; Lark et al., 2022).

As concerns the S-bearing liquid density calculation, sulfur was considered with M_i = 32.065 g mol^{-1} and with V_i = 20 $cm^3\ mol^{-1}$, although we do not exclude larger volumes. MMO liquid densities were computed considering different S contents (0, 1, 3, 5, 10 wt%) at an interval of 0.10 in the melt fraction F. Next, we determine the difference in density between the S-free and S-bearing MMO silicate liquids (called $\Delta\rho_{\mathrm{MMOs}}$) calculated as follows:

$$\Delta\rho_{\mathrm{MMOs}} = \rho_{\mathrm{MMO,S-free}} - \rho_{\mathrm{MMO,S-bearing}}$$

Where $\rho_{\mathrm{MMO,S\text{-}free}}$ is the density of the MMO liquid in S-free conditions and $\rho_{\mathrm{MMO,S\text{-}bearing}}$ is the density of the MMO liquid in S-bearing conditions (all expressed in kg m^{-3}). The $\Delta\rho_{\mathrm{MMOs}}$ values that we obtained are then plotted as a function of the S content in the MMO liquid (Fig. S12), where a linear relation was found:

$$\Delta\rho_{\mathrm{MMOs}} = 21.38\,[S]_{\mathrm{Melt}} \qquad (R^2 = 0.99)$$

Where $\Delta\rho_{\mathrm{MMOs}}$ is the density difference expressed in kg m^{-3}, and $[S]_{\mathrm{Melt}}$ is the concentration of sulfur in the melt expressed in wt%. As a first approximation, we assumed $\Delta\rho_{\mathrm{MMOs}}$ = 0 when no S is dissolved in the melt. We apply this correction to the S-free liquid density calculated with the EOS described in Section 3.1.

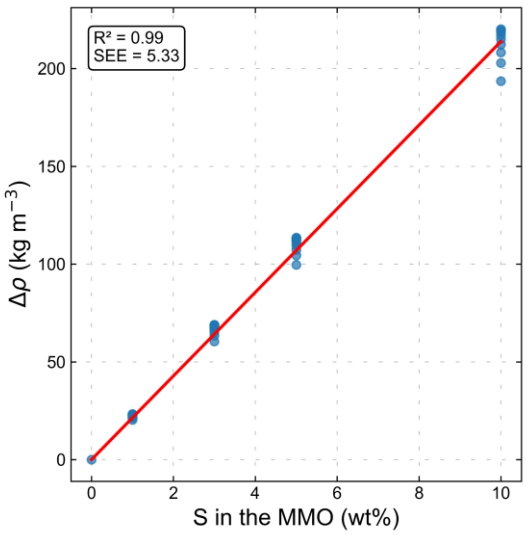

Figure S12: *Density difference between calculated S-free and S-bearing MMO liquids ($\Delta\rho_{\mathrm{MMOs}}$) as a function of the S content in the melt (expressed as wt%). The R^2 is 0.99 and the standard error of estimate (SEE) is 5.33 kg m^{-3}.*

S.13 HPE partitioning in the MMO

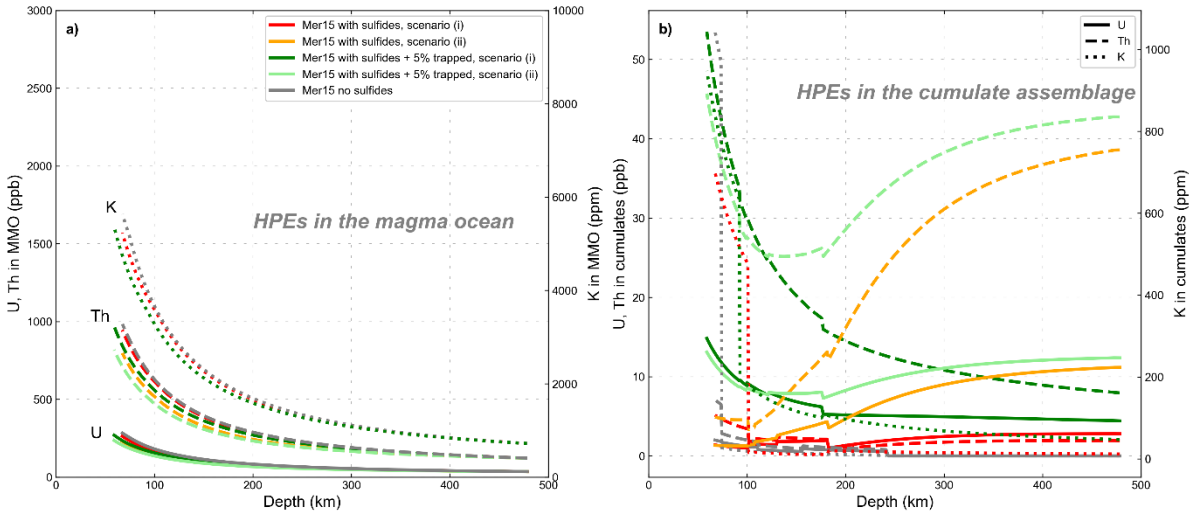

Figure S13: *(a) Uranium, thorium (both ppb), and potassium (ppm) distributions in the MMO as a function of depth (km) in Mer15. Grey lines refer to sulfide-free Mer15, red lines refer to sulfide-bearing Mer15 with incompatible HPEs (more details are in Section 6.5), orange lines refer to sulfide-bearing Mer15 with compatible HPEs, dark green lines refer to sulfide-bearing Mer15, incompatible HPEs with 5% trapped melt in the cumulate pile, and finally light green lines refer to sulfide-bearing Mer15, compatible HPEs with 5% trapped melt. Solid lines refer to uranium (U), dashed lines refer to thorium (Th), and dotted lines refer to potassium (K). (b) Uranium, thorium (both ppb), and potassium (ppm) distributions in the growing cumulates as a function of depth (km) in Mer15.*

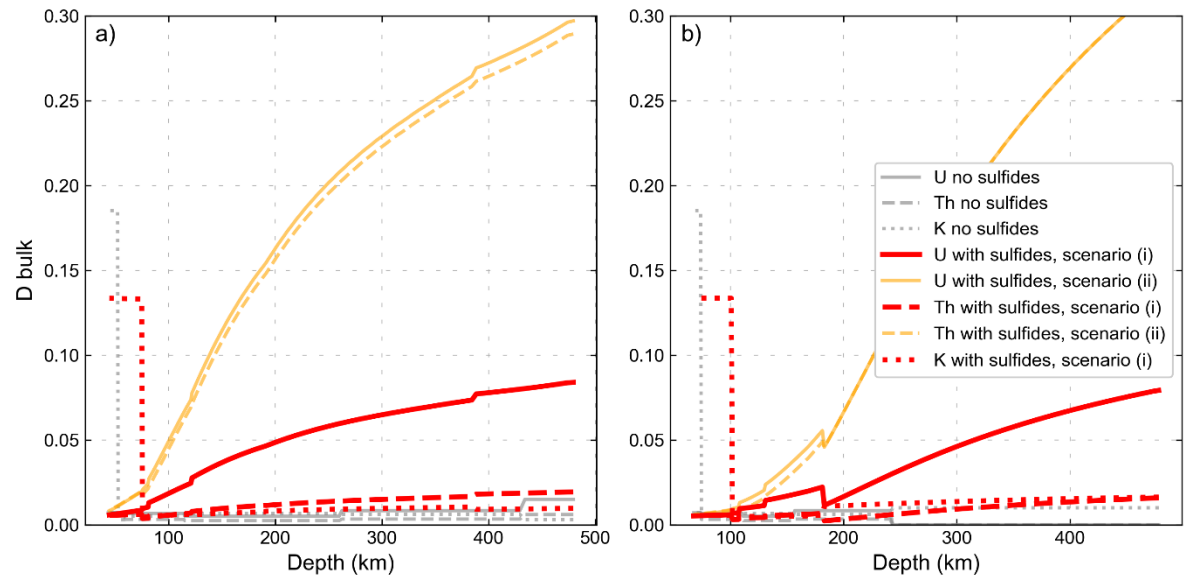

Figure S14: *Bulk partition coefficients D_{bulk} of U, Th, and K as a function of depth (km) for sulfide-free (grey lines), sulfide-bearing with incompatible HPEs (red lines), and sulfide-bearing with compatible HPEs (orange lines) for both (a) Mer8 and (b) Mer15.*

References

Baldwin, T.O., Tompson, C.W. (1964). X-ray characteristic temperatures of some II-VI ionic compounds. *The Journal of Chemical Physics* 41(5): 1420–1426. https://doi.org/10.1063/1.1726083

Bertka, C.M., Fei, Y. (1998). Density profile of an SNC model Martian interior and the moment-of-inertia factor of Mars. *Earth and Planetary Science Letters* 157: 79-88. https://doi.org/10.1016/S0012-821X(98)00030-2

Bottinga, Y., Richet, P., Weill, D.F. (1983). Calculation of the density and thermal expansion coefficient of silicate liquid. *Bulletin of Mineralogy* 106: 129-138.

Bottinga, Y., Weill, D.F. (1970). Density of liquid silicate systems calculated from partial molar volumes of oxide components. *American Journal of Science* 269: 169-182. https://doi.org/10.2475/ajs.269.2.169

Brown, S.M., Elkins-Tanton, L.T. (2009). Compositions of Mercury's earliest crust from magma ocean models. *Earth and Planetary Science Letters* 286: 446–455. https://doi.org/10.1016/j.epsl.2009.07.010

Charlier, B., Grove, T.L., Zuber, M.T. (2013). Phase equilibria of ultramafic compositions on Mercury and the origin of the compositional dichotomy. *Earth and Planetary Science Letters* 363: 50–60. https://doi.org/10.1016/j.epsl.2012.12.021

Fei, Y., Saxena, S.K., Navrotsky, A. (1990). Internally consistent thermodynamic data and equilibrium phase relations for compounds in the system MgO-SiO_2 at high pressure and high temperature. *Journal of Geophysical Research: Solid Earth* 95: 6915-6928. https://doi.org/10.1029/JB095iB05p06915

Frondel, C. (1962). *The system of mineralogy: vol. III silica minerals*. John Wiley and Sons Inc.

Ghiorso, M.S. (2004). An equation of state for silicate melts. I. Formulation of a general model. *American Journal of Science* 304: 637–678. https://doi.org/10.2475/ajs.304.8-9.637

Hart, S.R., Zindler, A. (1986). In search of a bulk-Earth composition. *Chemical Geology* 57: 247–267. https://doi.org/10.1016/0009-2541(86)90053-7

Holland, T.J.B., Green, E.C.R., Powell, R. (2018). Melting of peridotites through to granites: a simple thermodynamic model in the system KNCFMASHTOCr. *Journal of Petrology* 59: 881–900. https://doi.org/10.1093/petrology/egy048

Holland, T.J.B., Powell, R. (1998). An internally consistent thermodynamic data set for phases of petrological interest. *Journal of Metamorphic Geology* 16: 309-343.

Katz, R.F., Spiegelman, M., Langmuir, C.H. (2003). A new parameterization of hydrous mantle melting. *Geochemistry Geophysics Geosystems* 4: 1073. https://doi.org/10.1029/2002gc000433

Kosinski, J.A., Gualtieri, J.G., Ballato, A. (1992). Thermoelastic coefficients of alpha quartz. *IEEE Transactions on Ultrasonics, Ferroelectrics, and Frequency Control* 39: 502–507. 10.1109/58.148541. 10.1109/58.148541

Kushiro, I. (1969). The system forsterite-diopside-silica with and without water at high pressures. *American Journal of Science* 267-A: 269–294. https://doi.org/10.2475/001c.125224

Lange, R., Carmichael, I.S.E. (1987). Densities of Na_2O-K_2O-MgO-MgO-FeO-Fe_2O_3-Al_2O_3-TiO_2-SiO_2 liquids: new measurements and derived partial molar properties. *Geochimica et Cosmochimica Acta* 51: 2931–2946. https://doi.org/10.1016/0016-7037(87)90368-1

Lark, L.H., Parman, S., Huber, C., Parmentier, E.M., Head, J.W. (2022). Sulfides in Mercury's mantle: implications for Mercury's interior as interpreted from moment of inertia. *Geophysical Research Letters* 49: e2021GL096713. https://doi.org/10.1029/2021GL096713

Lauretta, D.S., Goreva, J.S., Hill, D.H., Killgore, M. (2007). Bulk compositions of the CB chondrites Bencubbin, Fountain Hills, MAC 02675, and MIL 05082. Lunar and Planetary Institute Conference Abstracts 38: 2236.

Morgan, J.W., Anders, E. (1980). Chemical composition of Earth, Venus, and Mercury. *Proceedings of the National Academy of Sciences USA* 77: 6973–6977. https://doi.org/10.1073/pnas.77.12.6973

Mouser, M. D., Dygert, N. (2023). On the potential for cumulate mantle overturn in Mercury. *Journal of Geophysical Research: Planets* 128: e2023JE007739. https://doi.org/10.1029/2023JE007739

Namur, O., Charlier, B. (2017). Silicate mineralogy at the surface of Mercury. *Nature Geoscience* 10: 9–13. https://doi.org/10.1038/ngeo2860

Namur, O., Collinet, M., Charlier, B., Grove, T.L., Holtz, F., McCammon, C. (2016). Melting processes and mantle sources of lavas on Mercury. *Earth and Planetary Science Letters* 439: 117–128. https://doi.org/10.1016/j.epsl.2016.01.030

Niu, Y.L., Batiza, R. (1991). In situ densities of MORB melts and residual mantle - implications for buoyancy forces beneath midocean ridges. *Journal of Geology* 99: 767-775. https://doi.org/10.1086/629538

Peiris, S. M., Campbell, A. J., & Heinz, D. L. (1994). Compression of MgS to 54 GPa. *Journal of Physics and Chemistry of Solids* 55 (5): 413–419. https://doi.org/10.1016/0022-3697(94)90166-X

Riel, N., Kaus, B.J.P., Green, E.C.R., Berlie, N. (2022). MAGEMin, an efficient Gibbs energy minimizer: application to igneous systems. *Geochemistry Geophysics Geosystems* 23: e2022GC010427. https://doi.org/10.1029/2022gc010427

Riner, M.A., Bina, C.R., Robinson, M.S., Desch, S.J. (2008). Internal structure of Mercury: implications of a molten core. *Journal of Geophysical Research: Planets* 113: 2007JE002993. https://doi.org/10.1029/2007JE002993

Robie, R.A., Hemingway, B.S. (1995). Thermodynamic properties of minerals and related substances at 298.15 K and 1 bar (105 Pascals) pressure and at higher temperatures. *U.S. Geological Survey Bulletin* 2131. https://doi.org/10.3133/b2131

Saracino, F., Charlier, B., Zhang, Y., Lécaille, M., Lin, Y., Namur, O. (2025). The role of sulfur on the liquidus temperature and olivine-orthopyroxene equilibria in highly reduced magmas. *Chemical Geology* 683: 122777. https://doi.org/10.1016/j.chemgeo.2025.122777

Singman, C.N. (1984). Atomic volume and allotropy of the elements. *Journal of Chemical Education* 61(2): 137. https://doi.org/10.1021/ed061p137

Toplis, M.J., Dingwell, D., Libourel, G. (1994). The effect of phosphorus on the iron redox ratio, viscosity, and density of an evolved ferrobasalt. *Contributions to Mineralogy and Petrology* 117: 293–304. https://doi.org/10.1007/BF00310870

Warren, P.H. (1995). Extrapolated partial molar densities of S03, P205, and other oxides in silicate melts. *American Mineralogist* 80: 1085–1088. https://doi.org/10.2138/am-1995-9-1027

Weisberg, M.K., Prinz, M., Clayton, R.N., Mayeda, T.K., Sugiura, N., Zashu, S., Ebihara, M. (2001). A new metal-rich chondrite grouplet. *Meteoritics and Planetary Science* 36: 401–418. https://doi.org/10.1111/j.1945-5100.2001.tb01882.x

Weisberg, M.K., Prinz, M., Humayun, M., Campbell, A.J. (2000). Origin of metal in the CB (Bencubbinite) chondrites. Lunar and Planetary Institute Conference Abstracts 31: 1466.

Weng, Y.-H., Presnall, D.C. (2001). The system diopside forsterite enstatite at 5.1 GPa: a ternary model for melting of the mantle. *The Canadian Mineralogist* 39: 299–308. https://doi.org/10.2113/gscanmin.39.2.299

Xu, Y., Lin, Y., Wu, P., Namur, O., Zhang, Y., Charlier, B. (2024). A diamond-bearing core-mantle boundary on Mercury. *Nature Communications* 15: 5061. https://doi.org/10.1038/s41467-024-49305-x